Continental Shelf Research 60 (2013) 17–27

Contents lists available at SciVerse ScienceDirect

Continental Shelf Research

journal homepage: www.elsevier.com/locate/csr

Research papers

Modeling tidal sand wave formation in a numerical shallow water model: The role of turbulence formulation

B.W. Borsje [a,b,*], P.C. Roos [a], W.M. Kranenburg [a], S.J.M.H. Hulscher [a]

[a] Water Engineering and Management, University of Twente, PO Box 217, 7500 AE Enschede, The Netherlands
[b] Deltares, Marine and Coastal Systems, Rotterdamseweg 185, PO Box 177, 2600 MH Delft, The Netherlands

ARTICLE INFO

Article history:
Received 24 January 2012
Received in revised form
9 April 2013
Accepted 12 April 2013
Available online 21 April 2013

Keywords:
Morphological/morphodynamic modeling
Tidal sand waves
Turbulence formulation
Delft3D
North Sea

ABSTRACT

Tidal sand waves are prominent dynamic bottom features in shallow sandy seas. Up to now, the processes controlling the formation of these bedforms have only been studied in stability sand wave models, in which geometry, boundary conditions and turbulence models are schematized. In this paper we present simulations of sand wave formation and migration with a numerical shallow water model (Delft3D), in which we restrict us to bedload transport and analyse the initial formation stage only. First, it is shown that the reproduction of the basic sand wave formation mechanisms in a numerical shallow water model requires careful treatment of model geometry, initial profile, vertical resolution and lateral boundary conditions. Second, an intercomparison between the Delft3D model and a nonlinear stability sand wave model is performed. Next, we compare the results for two of the built-in turbulence models: constant vertical eddy viscosity model (commonly used in stability sand wave models) and a more advanced spatially and temporally variable vertical eddy viscosity model (k–ε turbulence model). Finally, the model results are compared with field data on sand wave length. The k–ε turbulence model shows good agreement with the field data, whereas the constant vertical eddy viscosity model overestimates the wave length of the sand waves considerably.

1. Introduction

Large parts of the sandy seabed of shallow seas are covered with rhythmic bed patterns (Huntley et al., 1993). These bed patterns are the result of the complex interaction between hydrodynamics, sediment transport and morphology. The most dynamic large scale bed patterns are tidal sand waves, which regenerate in several years time (e.g. after dredging, see Knaapen and Hulscher (2002)), may grow up to 25% of the water depth (McCave, 1971), have wave lengths (distance between two successive crests) in the order of hundreds of meters (Van Dijk and Kleinhans, 2005) and migrate at a speed up to tens of meters per year (Terwindt, 1971; Dorst et al., 2009).

Given their dynamic behavior, sand waves may pose a hazard to offshore activities, by reducing the water depth of navigation channels, exposing pipelines and telecommunication cables and scouring offshore platforms or wind turbines (Németh et al., 2003). Consequently, insight in the processes controlling the variation in tidal sand wave characteristics is essential for cost-effective management practices.

Hulscher (1996) showed that sand wave formation can be explained as an inherent instability of the sandy seabed subject to tidal motion. The interaction of the oscillatory tidal current with a bottom perturbation gives rise to a tide-averaged residual circulation directed from the trough towards the crest of the sand wave. This residual circulation induces a net sediment flux towards the crest of sand waves, which leads to sand wave growth if the sediment transport overcomes the opposing effect of gravity. It is this competition between destabilizing and stabilizing sediment fluxes that defines a preferred wave length, termed the fastest growing mode (fgm). The model by Hulscher (1996) describes the hydrodynamics by using the three-dimensional shallow water equations. The turbulent stresses are accounted for by combining a constant vertical eddy viscosity with a partial slip condition at the bed. Sediment transport is only modeled as bedload transport. Despite the strongly schematized representation of the physical processes, the occurrence of sand waves in the Southern North Sea was predicted reasonably (Hulscher and Van den Brink, 2001). Later, Komarova and Hulscher (2000) extended

* Corresponding author at: Water Engineering and Management, University of Twente, PO Box 217, 7500 AE Enschede, The Netherlands. Tel.: +31 53 489 3546; fax: +31 53 489 5377.
E-mail addresses: b.w.borsje@utwente.nl (B.W. Borsje), p.c.roos@utwente.nl (P.C. Roos), w.m.kranenburg@utwente.nl (W.M. Kranenburg), s.j.m.h.hulscher@utwente.nl (S.J.M.H. Hulscher).

0278-4343/$ - see front matter © 2013 Elsevier Ltd. All rights reserved.
http://dx.doi.org/10.1016/j.csr.2013.04.023

the model of Hulscher (1996) by introducing a time dependency in the vertical eddy viscosity while keeping a partial slip condition at the bed. Moreover, Gerkema (2000) and Besio et al. (2003) improved the model of Hulscher (1996) by focusing on the hydrodynamic solution method. To explain sand wave migration, Németh et al. (2002) and Besio et al. (2004) introduced a residual current and tidal asymmetry, respectively, while keeping the simplified turbulence model. Blondeaux and Vittori (2005a, 2005b) and Besio et al. (2006) improved the model proposed by Hulscher (1996) by introducing a depth dependent eddy viscosity in combination with a no-slip condition at the bed. Moreover, both bedload transport and suspended load transport were included in the model. The model was able to reproduce the sand wave length at different locations on the Belgium Continental Shelf fairly well (Cherlet et al., 2007).

All the models discussed above are based on a linear stability analysis. In a linear stability analysis the growth rate of different infinitesimal perturbations is determined and the perturbation with the fastest growing mode is assumed to prevail. The model validity is thus limited to small-amplitude sand waves. Therefore, Németh et al. (2007) and Van den Berg et al. (2012) proposed a nonlinear stability sand wave model in which the sand wave behavior is modeled from its initial stage until an equilibrium shape. In both models a constant vertical eddy viscosity in combination with a partial slip condition at the bed is adopted. The model of Van den Berg et al. (2012) was able to reproduce the final sand wave length, height and shape at different locations in the Golden Gate region fairly well (Sterlini et al., 2009). However, the migration rates were largely overestimated by the model.

In this paper we explore the possibility to study sand wave formation in a numerical shallow water model. The advantage of such a model approach is that many physical processes can be included in a sophisticated way (e.g. wind- and wave-driven currents, density gradients, sediment transport, advanced turbulence models). However, given the high spatial and temporal resolution required to model tidal sand wave formation, these models require large computational effort. Also, treatment of lateral boundary conditions requires care. So far, the only study in which a numerical shallow model was used to investigate morphodynamic behavior of a sand wave was done by Tonnon et al. (2007). Their study focused on one artificial sand wave with an amplitude of 3 m, which makes it difficult to understand the processes controlling the formation of natural sand wave patterns.

In this study, we use the numerical shallow water model Delft3D with a schematized geometry and focus on small-amplitude sand waves. Consequently, in this paper we only study the initial stage of sand wave formation. In the Delft3D model, different turbulence closure models are built-in. The constant vertical eddy viscosity model is used to make an intercomparison between the Delft3D model and a nonlinear stability sand wave model (Van den Berg et al., 2012). The k–ε turbulence model allows the eddy viscosity to vary both in time and space and is used to determine the role of turbulence formulation on sand wave formation. As pointed out by Besio et al. (2006), the main improvement in the simplified description of sand wave formation in stability sand wave models would be a better turbulence model capable of describing the time variation of turbulence.

The aim of this paper is twofold. First, we aim to reproduce the initial stage of sand wave formation with a numerical shallow water model. Second, we aim to compare two of the built-in turbulence models: constant vertical eddy viscosity and k–ε and the effect on sand wave formation and migration. A comparison of the model results with field measurements on the wave length of sand wave fields in the Southern North Sea is provided.

The outline of this paper is as follows. First, the Delft3D model set-up is given, including model equations, boundary conditions and geometry (Section 2). Next, model results are presented with specific attention for the residual circulation and the growth rates. Moreover, the residual circulation obtained with the Delft3D model is compared with the residual circulation obtained with the nonlinear stability sand wave model of Van den Berg et al. (2012). Subsequently, the impact of both the constant vertical eddy viscosity model and the k–ε turbulence model on the preferred sand wave length and migration rate is presented (Section 3). The model results for both turbulence formulations are compared with sand wave lengths as observed in the Southern North Sea (Section 4). Section 5 discusses the main findings of this paper, focusing on the similarities and differences between the model results of the Delft3D model and the stability sand wave models. Finally, the conclusions are given (Section 6).

2. Model description

2.1. Hydrodynamics

The formation of sand waves is modeled using the numerical shallow water model Delft3D-FLOW (Lesser et al., 2004). The system of equations consists of the horizontal momentum equations, a continuity equation, a turbulence closure model, a sediment transport equation and a sediment continuity equation. The vertical momentum equation is reduced to the hydrostatic pressure relation as vertical accelerations are assumed to be small compared to gravitational acceleration. The model equations are solved by applying sigma layering in the vertical (Deltares, 2013). In this study, the model is run in the 2DV mode, i.e. considering flow and variation in x and z direction only, while assuming zero flow and uniformity in y direction and ignoring Coriolis effects. At the length scales of sand waves, Coriolis effects are assumed to have a negligible effect (Hulscher, 1996).

In terms of the σ-coordinates, the 2DV hydrostatic shallow water equations are described by

$$\frac{\partial u}{\partial t}+u\frac{\partial u}{\partial x}+\frac{\omega}{(H+\zeta)}\frac{\partial u}{\partial \sigma}=-\frac{1}{\rho_w}P_u+F_u+\frac{1}{(H+\zeta)^2}\frac{\partial}{\partial \sigma}\left(\upsilon\frac{\partial u}{\partial \sigma}\right), \tag{1}$$

$$\frac{\partial \omega}{\partial \sigma}=-\frac{\partial \zeta}{\partial t}-\frac{[(H+\zeta)\mu]}{\partial x}. \tag{2}$$

here u is the horizontal velocity, ω is vertical velocity relative to the moving vertical σ-plane, ρ_w is the water density, H is water depth below reference datum, ζ is the free surface elevation, P_u is the pressure gradient, F_u is the horizontal Reynolds stress and υ is the vertical eddy viscosity.

Two different turbulence models are used in the simulations presented in this paper. The first turbulence model assumes a constant value for the vertical eddy viscosity υ both in time and space (Eq. (3)A: Fredsøe and Deigaard, 1992). The second turbulence model is the more advanced k–ε turbulence closure model in which both the turbulent energy k and the dissipation rate ε are computed (Eq. (3)B: Rodi, 1984). The resulting vertical eddy viscosity υ is variable both in time and space (for details on the k–ε turbulence model formulations see Burchard et al., 2008):

$$\text{(A)}\quad \upsilon=\frac{\kappa U H_0\sqrt{g}}{6C},\quad \text{(B)}\quad \upsilon=c_\mu\frac{k^2}{\varepsilon} \tag{3}$$

in which κ is the von kármán constant (0.41), U is the amplitude of the depth-averaged flow velocity, H_0 is the mean water depth, g is the gravitational acceleration, C is the Chézy roughness coefficient and c_μ is set equal to 0.09 (Rodi, 1984).

At the bed ($\sigma=-1$), a quadratic friction law is applied and the vertical velocity ω is set to zero:

$$\tau_b \equiv \rho_w \frac{\upsilon}{(H+\zeta)}\frac{\partial u}{\partial \sigma} = \rho_w u_* |u_*| \qquad \omega = 0, \tag{4}$$

in which τ_b is the bed shear stress and u_* is the shear velocity, that relates the velocity gradient at the bed to the velocity u in the lowest computational grid point by assuming a logarithmic velocity profile (Deltares, 2013).

At the free surface ($\sigma=0$), a no-stress condition is applied and the vertical velocity ω is set to zero:

$$\rho_w \frac{\upsilon}{(H+\zeta)}\frac{\partial u}{\partial \sigma} = 0, \qquad \omega = 0, \tag{5}$$

2.2. Sediment transport and bed evolution

The bedload transport, S_b is calculated by

$$S_b = 0.006 \alpha_s \rho_s w_s d\, M^{0.5} M_e^{0.7}, \tag{6}$$

where α_s is a correction parameter for the slope effects (see below), ρ_s is the density of the sediment, w_s is the settling velocity of the sediment and d the sediment grain size. The sediment mobility number M and the excess sediment mobility number M_e are given by

$$M = \frac{u_r^2}{(\rho_s/\rho_w - 1) g d}, \qquad M_e = \frac{(u_r - u_{cr})^2}{(\rho_s/\rho_w - 1) g d}, \tag{7}$$

where u_r is the magnitude of the equivalent depth-averaged velocity computed from the velocity in the bottom computational layer assuming a logarithmic velocity profile and u_{cr} is the critical depth-averaged velocity for the initiation of motion of sediment based on the Shields curve. If $u_r < u_{cr}$ the bedload transport is set to zero.

Bedload transport is affected by bed level gradients, which makes sediment transported downhill more easily than uphill. Following Bagnold (1956), the correction parameter α_s for the slope effect is given by

$$\alpha_s = \lambda_s, \tag{8}$$

where λ_s is the slope parameter which is usually taken inversely proportional to the tangent of the angle of repose of sand (Sekine and Parker, 1992). The angle of repose of sand is in the range between 15° and 30°. In this paper we set λ_s equal to 2.5, following van den Berg et al. (2012).

Finally, the bed evolution is governed by the sediment continuity equation (Exner equation), which reads

$$(1-\varepsilon_p)\frac{\partial z_b}{\partial t} + \frac{\partial S_b}{\partial x} = 0, \tag{9}$$

in which z_b is the bed level and $\varepsilon_p=0.4$ is the bed porosity. Eq. (9) simply states that convergence (or divergence) of the bedload transport rate must be accompanied by a rise (or fall) of the bed profile.

2.3. Model set-up

In the horizontal, the model domain is 50 km, with a variable horizontal resolution. In the centre of the model domain the grid size is 10 m, increasing to a value of 1500 m at the lateral boundaries. In the vertical, the model grid is composed of 20 layers, with small vertical resolution near the bed and increasing towards the water surface. At the lateral boundaries, a so-called Riemann boundary condition is imposed (Verboom and Slob, 1984). For this type of boundary condition, outgoing waves are allowed to cross the open boundary without being reflected back into the computational domain, as happens for other type of boundary conditions. The semi-diurnal depth-averaged velocity amplitude U_{M2} at these lateral boundaries is set at $U_{M2}=0.65$ m s^{-1}

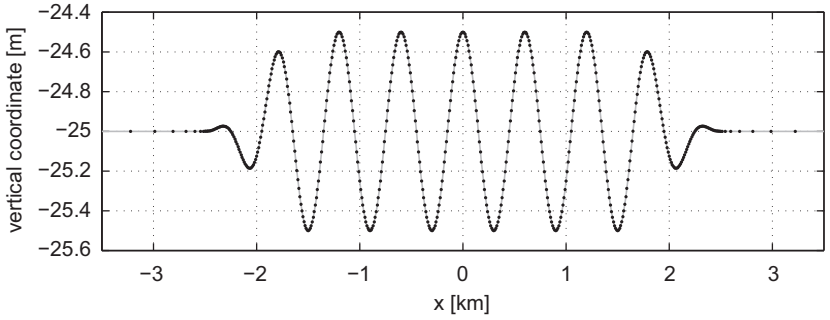

Fig. 1. Initial bed level for a sand wave field with a wave length $L=600$ m. The crest of the central sand wave is located at $x=0$. The total model domain is 50 km. Horizontal grid points are indicated with circles.

Table 1
Overview of the default values and dimensions of the model parameters.

Description	Symbol	Value(s)			Dimension
Physics:					
Tidal frequency of M_2-tide	σ_{M2}	1.45×10^{-4}			s^{-1}
Mean water depth	H_0	25			m
Sediment grain size	d	0.35			mm
Sand wave length	L	[160–4500]			m
Tidal conditions:		I	II	III	
Amplitude of horizontal M_2-tidal velocity	U_{M2}	0.65	0.65	0.65	m s^{-1}
Residual current M_0	U_{M0}	0	0.05	0	m s^{-1}
Amplitude of horizontal M_4-tidal velocity	U_{M4}	0	0	0.05	m s^{-1}
Phase lag between M_2 and M_4	Φ	–	–	120	°

and the tidal frequency $\sigma_{M2}=1.45\times10^{-4}$ s^{-1}. The depth-averaged velocity amplitude is imposed with a logarithmic vertical profile at the lateral boundary. The initial bed level perturbation z_b is prescribed by a multiplication of a sinusoidal sand wave pattern ($z_b=A(t)\exp(2\pi ix/L)+$ c.c.) of a given wave length L and amplitude A with an envelope function, ensuring a gradual transition from the flat bed towards the sand wave field in the centre of the domain (Fig. 1). Consequently, a coarser grid can be used near the boundaries. The mean water depth $H_0=25$ m and the sediment grain size $d=0.35$ mm. The setting for flow velocity amplitude, mean water depth and grain size resemble a typical North Sea situation for sand wave occurrence (Borsje et al., 2009). The Chézy

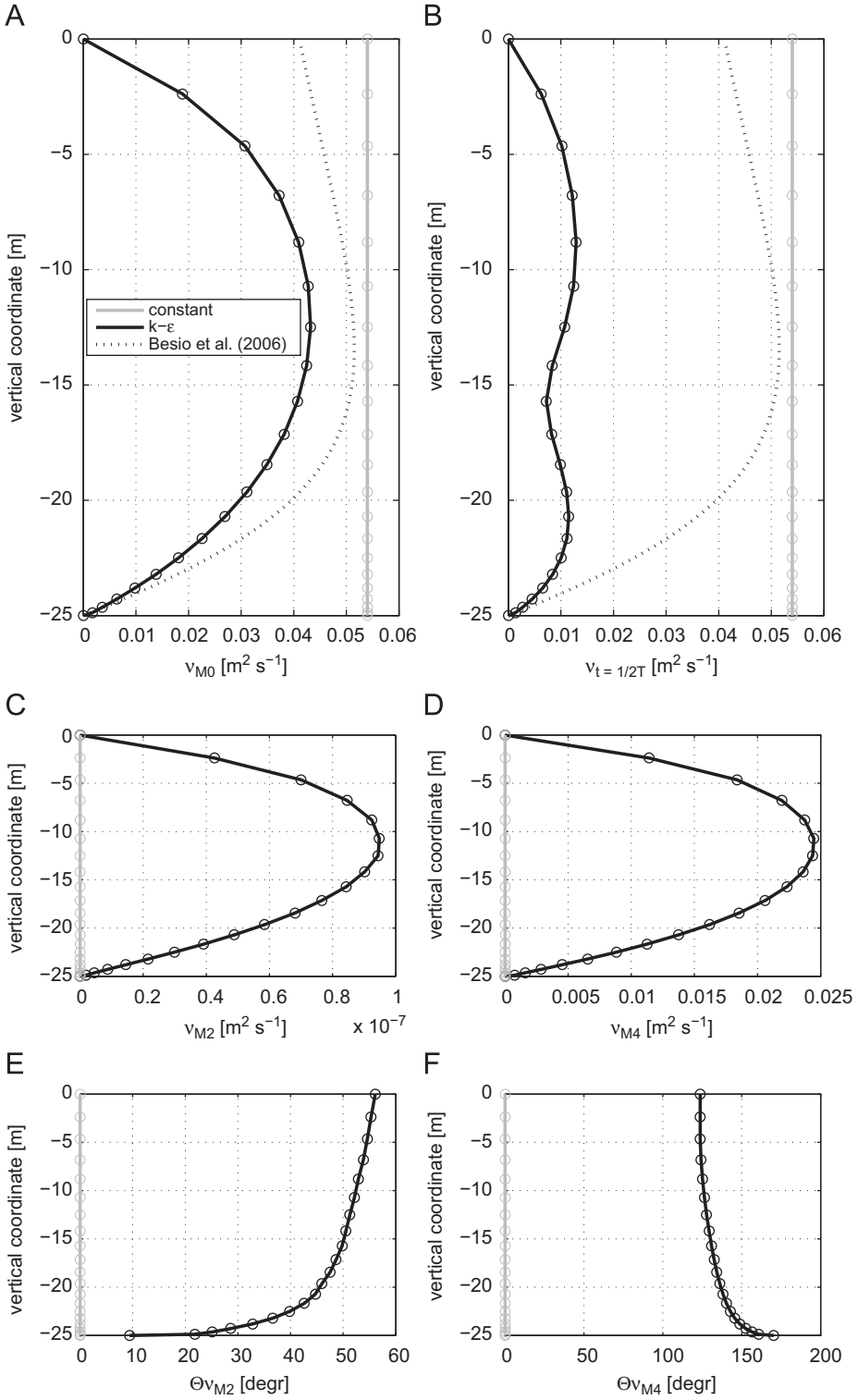

Fig. 2. Eddy viscosity profiles υ [m^2 s^{-1}] for the constant vertical eddy viscosity model (gray line) and the k–ε turbulence model (black line). Tide-averaged values of the eddy viscosity υ_{M0} [m^2 s^{-1}] (A), instant values of the eddy viscosity during flow reversal ($t=\frac{1}{2}T$) (B), the first (C) and second (D) harmonic eddy viscosity component υ_{M4} [m^2 s^{-1}] and phases Θ_{M2} [degr] (E) and Θ_{M4} [degr] (F) for a flat bed. (Case I in Table 1). Eddy viscosity profile υ [m^2 s^{-1}] for the model by Besio et al. (2006) is included for later reference.

roughness coefficient C is set equal to 65 $m^{1/2}$ s^{-1}, following Tonnon et al. (2007). The initial amplitude of the sand wave A_0=0.5 m. The model is run for two tidal cycles. The first tidal cycle is used for spin-up and no bed level changes are computed during this period. The second tidal cycle is used for determining the bed evolution. All default parameter settings are listed in Table 1. The sets of tidal conditions will be referred to in Section 3.

3. Results

3.1. Hydrodynamics

First, we study the effect of the different turbulence models on the eddy viscosity profile and flow velocity profile for a flat bed. The flat bed serves as the basic state in stability sand wave model (Dodd et al., 2003). The eddy viscosity profile for the constant vertical eddy viscosity model shows a higher tide-averaged eddy viscosity υ_{M0}, compared to the k–ε turbulence model (Fig. 2A). In addition, the k–ε turbulence model also shows a time dependency in υ, which can be explained in a Fourier series according to

$$\upsilon = \upsilon_{M0}(z) + \upsilon_{M2}(z)\cos(\sigma t - \theta_{M2}(z)) + \upsilon_{M4}(z)\cos(2\sigma t - \theta_{M4}(z)) + \cdots \quad (10)$$

The most dominant component (the quarter-diurnal component) shows an amplitude of υ_{M4}=0.025 m^2 s^{-1} (Fig. 2D) and a phase θ_{M4} of around 120° (Fig. 2F).

Given the differences in eddy viscosity profiles, the flow velocity profiles are also different for the two turbulence models for a flat bed (Fig. 3). The tide-averaged flow velocity profiles U_{M0} both show small negative flow velocity amplitudes (Fig. 3A), which will be shown to be much smaller than the tide-averaged flow velocity profiles for a wavy bed (residual circulation cell). The dominant flow velocity component U_{M2} shows a larger near-bed velocity for the constant vertical eddy viscosity model compared to the k–ε turbulence model (Fig. 3B). The difference between the near-bed velocities for both turbulence models is due to the much larger viscosity near the bed for the constant vertical eddy viscosity model, compared to the k–ε turbulence model (Fig. 2A). Consequently, the gradient in flow velocity is much smaller for the constant vertical eddy viscosity model (Eq. (4)). As a result, the near-bed velocities for the k–ε turbulence model attain a much smaller value compared to the constant vertical eddy viscosity model.

Next, we replace the flat bed with a wavy bed with a wave length L=600 m in order to study the hydrodynamic response. As shown by Hulscher (1996), due to the interaction of the flow with the wavy bed, the tide-averaged residual sea level is 180° out of phase with the bottom perturbation. As a consequence, averaged over one tidal cycle, the flow velocity profiles show a residual circulation cell: tide-averaged flow velocities directed from the trough of the sand wave towards the crest near the bed for both turbulence models (Fig. 4).

Next, we compare the results of the Delft3D model with a nonlinear stability sand wave model (Van den Berg et al., 2012), focusing on the residual circulation cell. In both models a constant vertical eddy viscosity model is adopted. In the model of Van den Berg et al. (2012) the eddy viscosity υ, water depth H, wave length L, flow velocity amplitude U_{M2}, tidal frequency σ_{M2} and initial sand wave amplitude A_0 are chosen identically to our model set-up (Table 1; Case I). For all other parameter settings, the default parameters are taken (Van den Berg et al., 2012). Comparison of the tide-averaged flow velocity profile u_{M0} [m s^{-1}] at the flank for the Delft3D model (Fig. 4B; black line) with the nonlinear stability

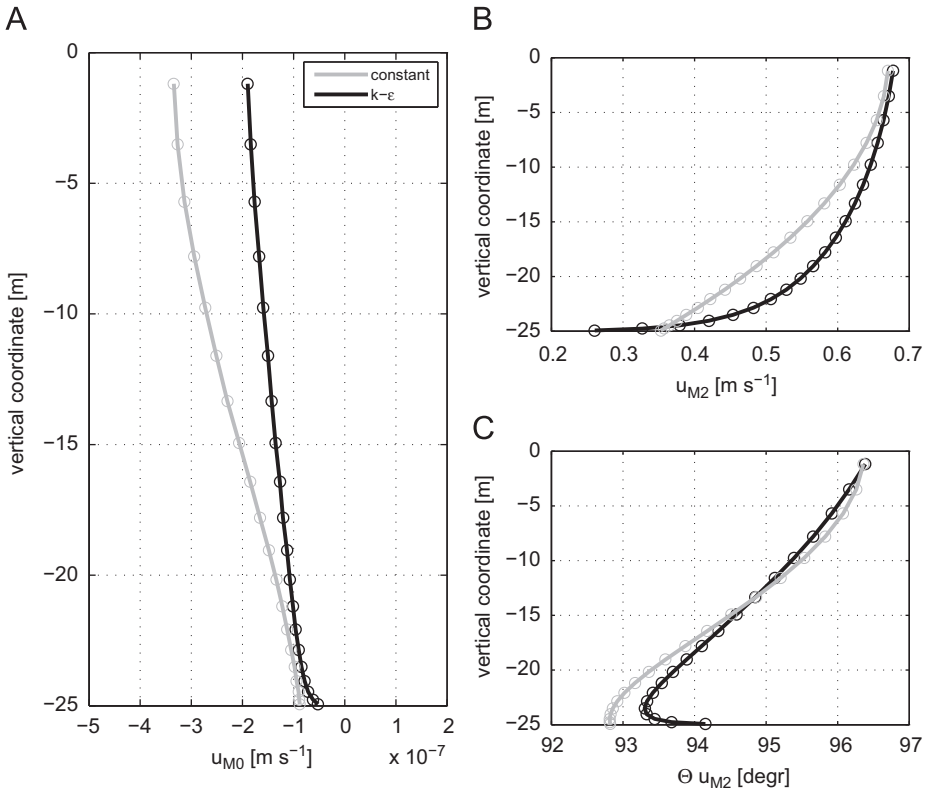

Fig. 3. Flow velocity profiles u [m s^{-1}] for the constant vertical eddy viscosity model (gray line) and the k–ε turbulence model (black line). Tide-averaged values of the flow velocity u_{M0} [m s^{-1}] (A) and the first harmonic flow velocity component u_{M2} [m s^{-1}] (B) and phase Θ u_{M2} [degr] (C) for a flat bed. (Case I in Table 1).

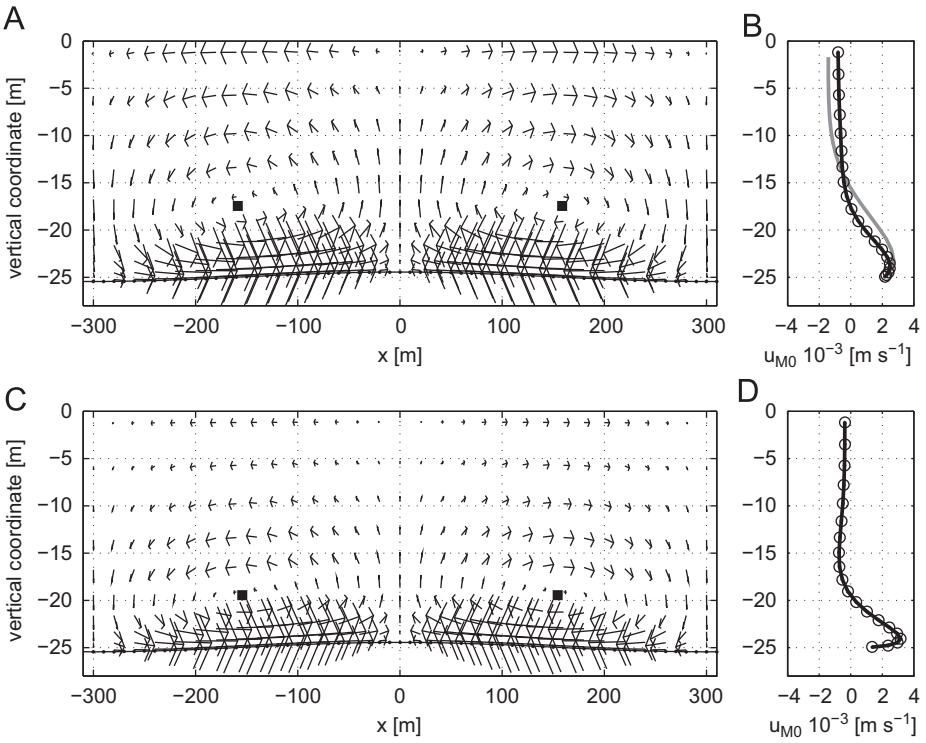

Fig. 4. Tide-averaged residual current over a sand wave with wave length L=600 m, for a simulation with the constant vertical eddy viscosity model (A) and the k–ϵ turbulence model (C). The centre of the residual circulation cell is indicated with a black square. Tide-averaged flow velocities profiles u_{M0} [m s^{-1}] are shown at the flank x=−L/4=−150 m for the constant vertical eddy viscosity (B) and k–ϵ turbulence model (D). (Case I in Table 1). The tide-averaged flow velocity profile u_{M0} [m s^{-1}] at the flank for the nonlinear stability sand wave model by Van den Berg et al. (2012) is shown with the gray line (B).

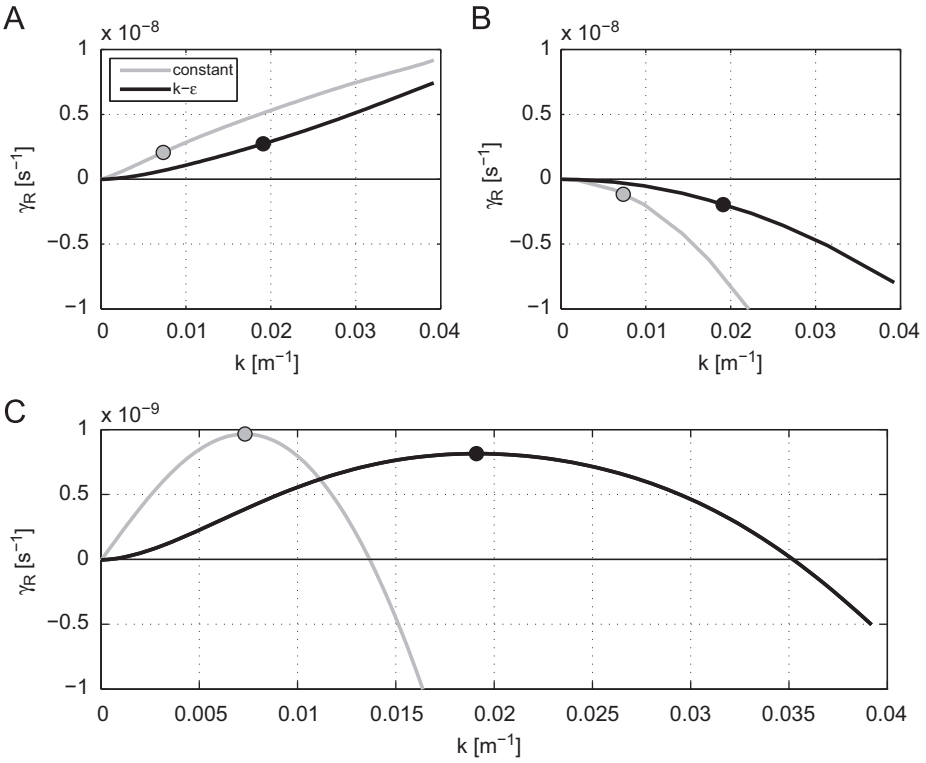

Fig. 5. The total growth rate curve (C) is the sum of the plain bedload transport component (A) and the slope-induced transport component (B). On the horizontal axis the wave number k [m^{-1}] is given and on the vertical axis the growth rate γ_R [s^{-1}]. The circles indicate the growth rates belonging to the fastest growing mode L_{fgm}. Two turbulence models are shown: constant vertical eddy viscosity (gray line) and k–ϵ turbulence model (black line). (Case I in Table 1).

sand wave model by Van den Berg et al. (2012) (Fig. 4B; gray line) shows fairly good agreement. Particularly, the tide-averaged flow velocity amplitudes near the bed coincide. In conclusion, the numerical shallow water model adopted in this paper is capable of reproducing the tide-averaged residual current as earlier found in the nonlinear stability sand wave model of Van den Berg et al. (2012).

Qualitatively, the residual circulation cells are similar for both turbulence models (Fig. 4). However, compared to the constant vertical eddy viscosity model, the k–ε turbulence model shows weaker near-bed velocities and the centre of the residual circulation cell is found closer near to the bed. The strength of the residual circulation cell is small compared to the amplitude of the tidal velocity. However, the strength of the tide-averaged flow velocity near the bed is much larger for the wavy bottom case (Fig. 4B and Fig. 4D), compared to the flat bed (Fig. 3A).

3.2. Bed evolution

Now let us investigate the growth rate as a function of the topographic wave number $k=2\pi/L$, for both turbulence models, and isolating the contributions due to the plain bedload transport (neglecting slope-induced transport) and the slope-induced transport (Case I Table 1). We have varied the wave length L in a range of 160 m till 4500 m (Table 1). Assuming exponential growth (which is valid for small-amplitude sand waves (Besio et al., 2008)), the growth rate γ_R for the bed perturbation is calculated by

$$\gamma_R = \frac{1}{T}\mathrm{Re}\left\{\log\left(\frac{A_1}{A_0}\right)\right\}, \tag{11}$$

where T is the tidal period, A_1 is the bed amplitude of the sand wave after one tidal cycle. A_0 and A_1 are determined by a fast Fourier transform (FFT) of the central part of the sand wave domain. Positive values of Y_R indicate growth of the bottom perturbation, whereas negative values indicate decay.

Given the direction of the tide-averaged near-bed velocities, a small net transport of sediment directed from the trough towards the crest of the sand wave is expected when slope-induced transport is neglected. For a given wave length of the sand wave, water depth and flow velocity amplitude, the strength of the residual circulation cell can be determined. In general, the sand wave with the largest wave number causes the strongest residual circulation cell. Consequently, neglecting the slope-induced transport, the sand wave with the smallest wave length shows the largest growth rate, for both turbulence models (Fig. 5A). However, the growth rate for the constant vertical eddy viscosity model is larger, due to the stronger tide-averaged near-bed velocities for a given wave number (Fig. 4).

Due to the slope effect, the sand wave tends to decay. The slope-induced transport is the strongest for large wave numbers. The slope of the bed form is equal for both simulations for a given wave number, but the magnitude of the transport rate is much larger for the constant vertical eddy viscosity model, resulting in a stronger slope-induced transport (Fig. 5B).

The total growth curve is the sum of the plain bedload transport and the slope-induced transport (Fig. 5C). The fastest growing mode is the wave number which triggers the fastest initial growth. In conclusion, the wave length for the fastest growing mode for the constant vertical eddy viscosity model is much larger ($L_{fgm}=870$ m), compared to the k–ε turbulence model ($L_{fgm}=330$ m).

3.3. Migration

For a symmetrical forcing, sand waves do not migrate. However, if a residual current U_{M0} or another tidal component (e.g. the quarter-diurnal M_4-tidal component) is present next to the semi-diurnal tidal component M_2, the sand waves may display migration (Németh et al., 2002; Besio et al., 2004). Typical values for the residual current U_{M0} and the amplitude of the M_4-tidal component U_{M4} are 0.05 m s^{-1} for the North Sea (Besio et al., 2004). The phase lag between the M_2 and M_4-tidal component determines the

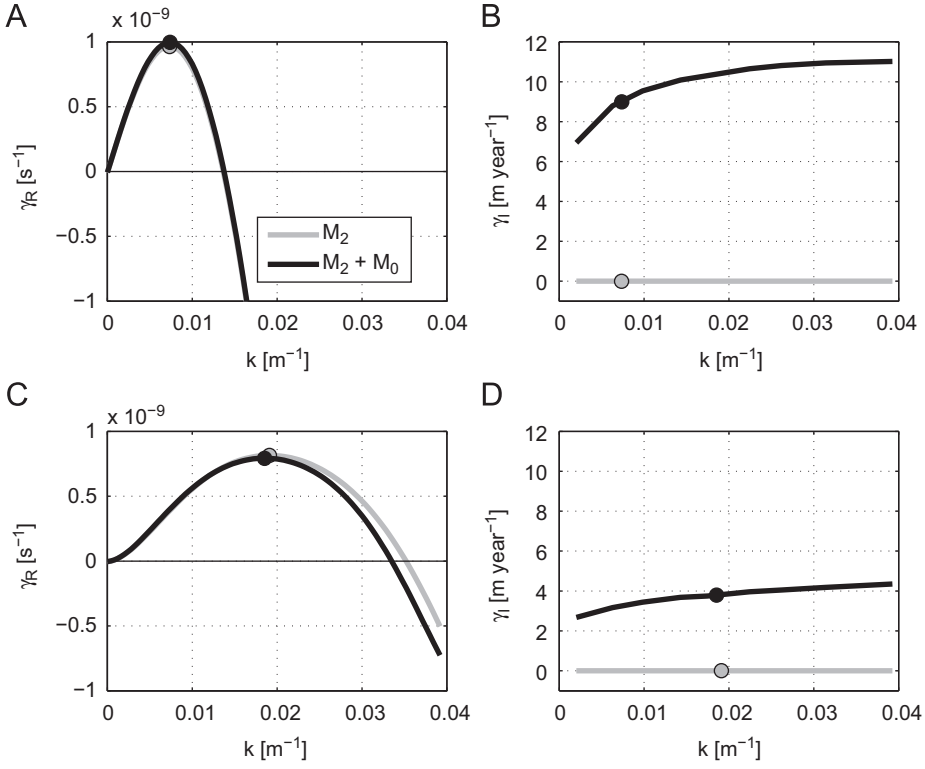

Fig. 6. Growth rate γ_R [s^{-1}] and migration rate γ_I [m year^{-1}] as a function of wave number k [m^{-1}], for constant vertical eddy viscosity (top) and k–ε (bottom). Distinction is made between only M_2 tidal forcing (gray line) and combined M_2 and M_0 tidal forcing (black line). The circles indicate the growth rates and migration rates belonging to the fastest growing modes L_{fgm}. (Case II in Table 1).

direction of migration (Besio et al., 2004), whereas the residual current causes sand waves to migrate always in the downstream direction (Németh et al., 2002). Besio et al. (2004) showed that for a phase lag of 120° between the M_2 and M_4-tidal component sand wave migration in the upstream direction is possible.

In this section we show the results for four simulations. The first two simulations are the inclusion of a residual current U_{M0} of 0.05 m s^{-1} on top of the default model settings (Case II in Table 1) for both turbulence models. The next two simulations are the inclusion of a M_4-tidal component of $U_{M4}=0.05$ m s^{-1} and a phase lag $\varphi=120°$ between the M_2 and M_4-tidal component for both turbulence models (Case III in Table 1). Sand wave migration implies that A_1 is a complex quantity (Besio et al., 2008). A_0 and A_1 are determined by a Fast Fourier Transform (FFT) of the central

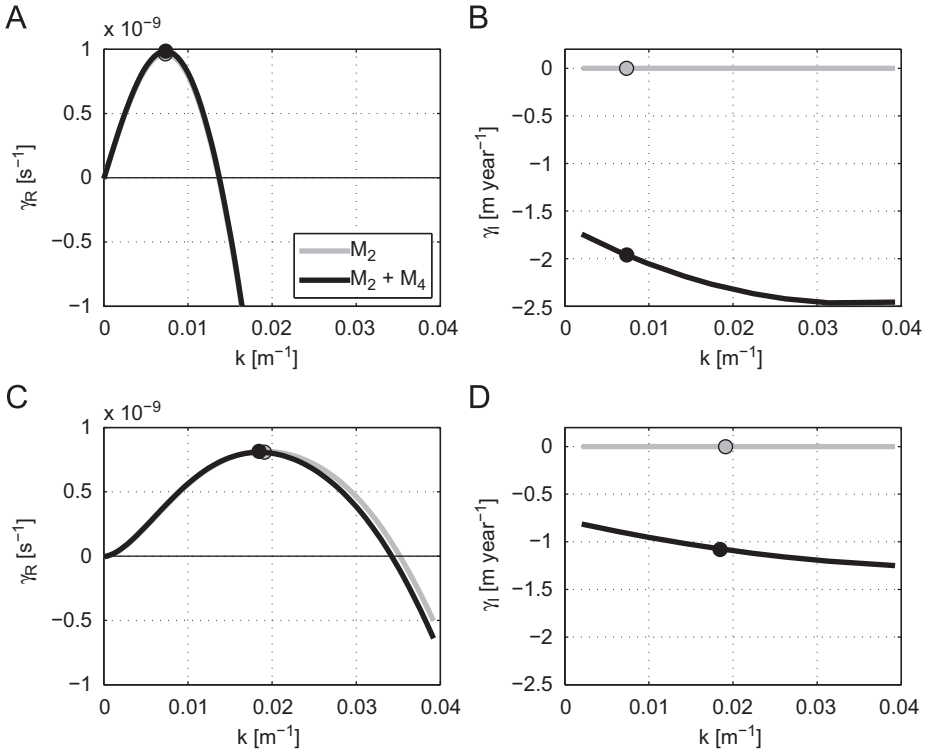

Fig. 7. Growth rate γ_R [s^{-1}] and migration rate γ_I [m year^{-1}] as a function of wave number k [m^{-1}], for constant vertical eddy viscosity (top) and k–ε (bottom). Distinction is made between only M_2 tidal forcing (gray line) and combined M_2 and M_4 tidal forcing (black line). The circles indicate the growth rates and migration rates belonging to the fastest growing modes L_{fgm}. (Case III in Table 1).

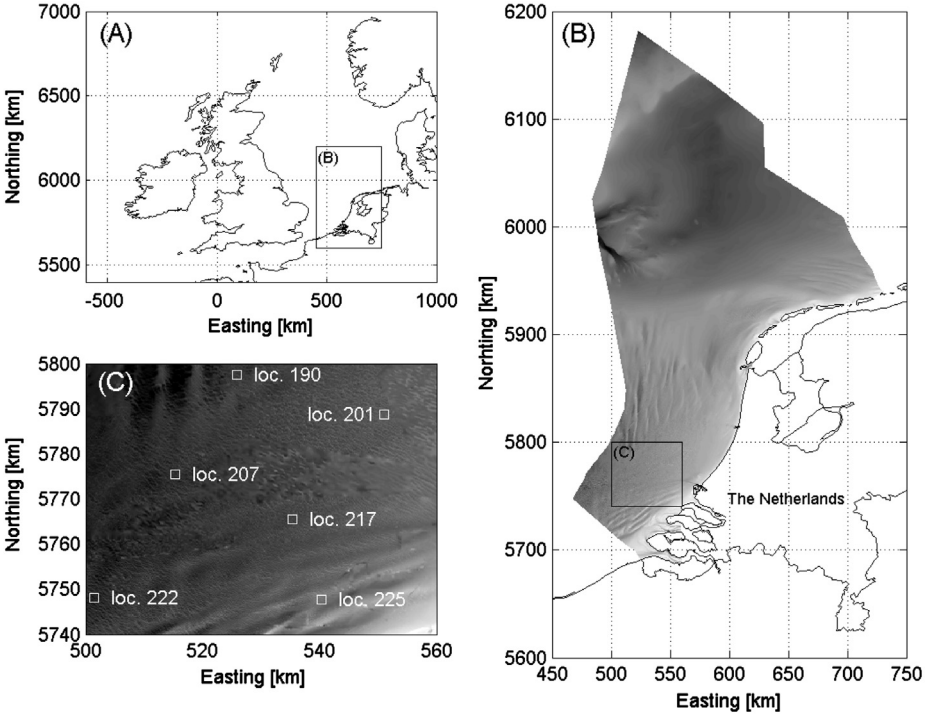

Fig. 8. Location of sand wave fields (C) used in the comparison of the model results, located in the Dutch part of the North Sea (B) in North-West Europe (A).

part of the sand wave domain. The migration rate γ_I of the sand wave is calculated by

$$\gamma_I = \frac{-1}{kT}\mathrm{Im}\left\{\log\left(\frac{A_1}{A_0}\right)\right\} \quad (12)$$

By including a residual current U_{M0}, the sand wave shows a positive migration rate, which means migration in the direction of the residual current. For the fastest growing mode the migration speed $\gamma_I = 9$ m year^{-1} for the constant vertical eddy viscosity model (Fig. 6B black circle), while for the k–ε turbulence model, the migration rate for the fastest growing mode $\gamma_I = 3.8$ m year^{-1} (Fig. 6D black circle). As expected, the migration rate for the symmetrical forcing (M_2-tidal component) is nearly zero (order of centimeters per year: Fig. 6B and D gray circles). The growth curves are nearly identical for both turbulence models (Fig. 6A and C), indicating that the inclusion of a small residual current will not change the strength of the residual circulation cell and hence the fastest growing mode. The larger migration rate for the constant vertical eddy viscosity model is caused by the larger transport rates compared to the k–ε turbulence model.

By including a M_4-tidal component with a phase lag $\varphi = 120^\circ$ with the M_2-tidal component, the sand wave show a negative migration rate, which means migration in the upstream direction (Fig. 7). For the fastest growing mode the migration speed $\gamma_I = -1.9$ m year^{-1} for the constant vertical eddy viscosity model (Fig. 7B black circle), while for the k–ε turbulence model, the migration rate for the fastest growing mode $\gamma_I = -1.1$ m year^{-1} (Fig. 7D black circle). Again, the migration rate for the symmetrical forcing (M_2) is nearly zero (Fig. 7B and D gray circles) and the growth curves are nearly identical for both turbulence models (Fig. 7A and C).

Table 2
Mean wave length L of sand wave fields at six locations in the Dutch part of the North Sea. Data on the amplitude of the flow velocity U_{M2}, mean water depth H_0, grain size d and mean wave length L are taken from Van Santen et al. (2011). Locations numbers correspond to the numbers shown in Fig. 8.

Location no.	U_{M2} (m s^{-1})	H_0 (m)	d (mm)	L (m)
'225'	0.70	21.33	0.36	220
'222'	0.73	34.63	0.34	490
'217'	0.68	29.30	0.27	290
'207'	0.72	31.51	0.28	320
'201'	0.64	25.70	0.36	400
'190'	0.65	30.59	0.32	290
Range	[0.64–0.73]	[21.33–34.63]	[0.27–0.36]	[220–490]
Mean	0.69	28.84	0.32	335

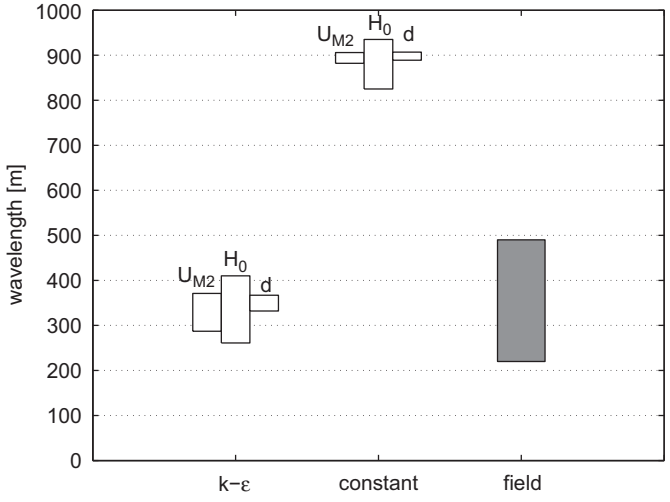

Fig. 9. Range in fastest growing mode for both turbulence models, by taking either the maximum or the minimum in flow velocity amplitude U_{M2}, mean water depth H_0 and grain size d while taking the mean of the other parameters (Table 2). The gray bar indicates the variation in wave length measured in the field, as provided by Van Santen et al. (2011).

4. Comparison of the model results with sand wave lengths in the Southern North Sea

The results of the model are compared with field data on sand wave length on the Dutch continental shelf (Fig. 8B). Comparison of the migration rates found in the model with field data is difficult, while the standard deviation in migration rates is in the same order as the average migration rate in the field (Besio et al., 2004). Nevertheless, the range in migration rates found in the simulations (Section 3.3) is comparable to field observations for the North Sea (Dorst et al., 2009).

Recently, Van Santen et al. (2011) presented an overview of 23 locations where sand waves are found on the Dutch continental shelf for which the flow velocity amplitude U_{M2}, grain size d, mean water depth H_0 and sand wave length L is given. Because we only study sand wave fields on top of a flat seabed in our model (Fig. 1), we selected six locations (Fig. 8C) which are not located on top of larger bedforms like sandbanks (Fig. 8B). As discussed by van Santen et al. (2011), the presence of larger bedforms is an important explanation for differences between model results and field observations.

The range in fastest growing mode is determined for both turbulence models by taking the mean of two of the three parameters and taking either the maximum or the minimum of the third parameter (Table 2). Based on a subset of the locations discussed by van Santen et al. (2011), it appears that the simulation in which the k–ε turbulence model is used agrees much better with the field data compared to the constant vertical eddy viscosity model (Fig. 9).

5. Discussion

This paper presents simulations with the numerical shallow water model Delft3D, in which the initial stage of sand wave formation has been reproduced. The formation of sand waves, extensively studied with stability sand wave models, has never been reproduced in a numerical shallow water model before. The main difficulty in reproducing sand wave formation in a numerical shallow water model is the reflection of the tidal wave by the imposed lateral boundary. In engineering practice, Delft3D is usually run with a flow velocity at one lateral boundary and a water level at the opposite lateral boundary (e.g. Tonnon et al., 2007). While these lateral boundary conditions are reflective, a small net tide-averaged current will be present in the modeling domain. The magnitude of this reflective net current is in the same order of magnitude as the net current induced by the bottom topography (see the residual circulation cells in Fig. 4). In this study, Riemann lateral boundary conditions have been used instead, in which outgoing waves can cross the open boundary without being reflected back into the computation domain.

The resolution used to reproduce sand wave formation is 10 m in horizontal direction in the sand wave domain and 20 layers in vertical direction, for which the layers close to the bed have a vertical resolution in the order of ten centimeters. The fine horizontal resolution is necessary to have enough grid cells to cover the smallest sand waves modeled ($L_{min} = 160$ m; Fig. 5). The fine vertical resolution is necessary to model the strong gradient in flow velocity profile near the bed (Fig. 4). A grid refinement study

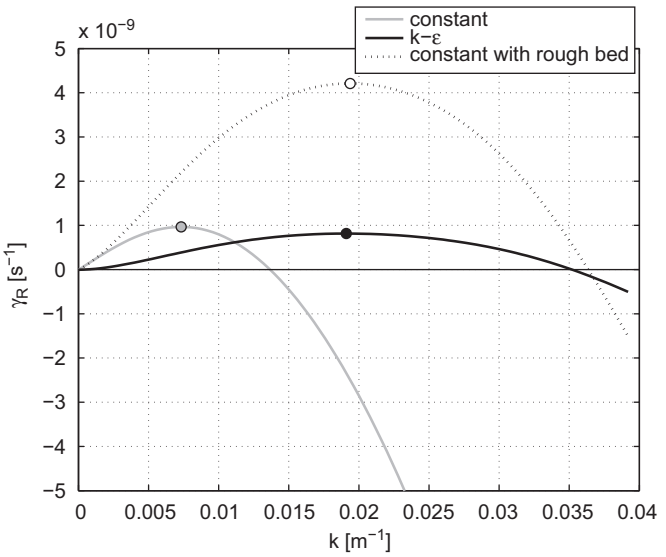

Fig. 10. Total growth curve and fastest growing mode for the constant vertical eddy viscosity model (gray line—gray circle), k–ε turbulence model (black line—black circle) and the constant vertical eddy viscosity model with a rough bed (black dashed line—white circle). Chézy roughness $C=65\ m^{1/2}\ s^{-1}$ and $C=48\ m^{1/2}\ s^{-1}$ for the default case and the rough bed case, respectively. (Case I in Table 1).

is conducted and illustrates that 20 vertical layers is sufficient to describe accurately the flow field (not shown).

The overestimation in wave length of sand waves by using a constant vertical eddy viscosity is often corrected for by increasing the bed roughness (e.g. Van Santen et al., 2011; Sterlini et al., 2009; Németh et al., 2002). An increase in bed roughness causes a steeper gradient in flow velocity near the bed, and therefore a flow velocity profile which matches the velocity profile calculated with the k–ε turbulence model better. Nevertheless, by increasing the roughness of the bed, both the bed shear stress and the bedload transport rate increase. Consequently, the fastest growing mode could be matched for the two different turbulence models (Fig. 10). However, by increasing the bed roughness, the migration rate will increase to unrealistic values, as discussed by Sterlini et al. (2009) and Németh et al. (2002), up to 150 m year^{-1}. Moreover, the bed roughness is not an independent parameter, the value depends on the grain size and, when ripples form, on hydrodynamic conditions. Therefore, correcting the overestimation in wave length for stability sand wave models with a constant vertical eddy viscosity by increasing the bed roughness will not only result in unrealistic high migration rates but is also physically incorrect.

The results of the numerical shallow water model are comparable to the results of stability sand wave models (Besio et al., 2008): sand waves with a wave length in the order of several hundreds of meters and migration rates in the order of some meters per year are found. However, the main difference between both type of models is the growth rate for sand waves near $k=0$ (Fig. 5C). The growth rate for very long sand waves is much smaller for the k–ε turbulence model, compared to the constant vertical eddy viscosity model. For a wavelength of e.g. $L=3000$ m the growth rate for the k–ε turbulence model is 10 times smaller, but still shows a positive growth rate (Fig. 5C).

As discussed in the introduction, Besio et al. (2006) improved the model proposed by Hulscher (1996) by introducing a depth dependent eddy viscosity in combination with a no-slip condition at the bed. The shape of the viscosity profile prescribed in the model by Besio et al. (2006) is comparable to the shape of the k–ε viscosity profile (Fig. 3A), nevertheless during flow reversal the viscosity profile for the Delft3D model and the model by Besio et al. (2006) deviates strongly (Fig. 3B). The impact of this difference on sand wave formation will be studied in future research, starting with the role of suspended sediment in combination with the time variation in eddy viscosity. Moreover, a next step is to run the model for a longer period and study the mechanisms which control the equilibrium shape of sand waves.

6. Conclusions

The initial stage of tidal sand wave formation was successfully reproduced in a numerical shallow water model (Delft3D). In order to resolve the tide-averaged residual current over a sand wave, non-reflective lateral boundaries and a high resolution both in time and space is needed.

The model was run with two turbulence models: constant vertical eddy viscosity and an advanced spatially and temporally variable vertical eddy viscosity model (k–ε turbulence model). For the same tidal conditions, the constant vertical eddy viscosity model showed higher tide-averaged near-bed velocities, and consequently causing longer sand waves and higher migration rates compared to the k–ε turbulence model.

Next, we compared field data on sand wave length of the southern North Sea with the results of both turbulence models. For the sites considered, the k–ε turbulence model showed good agreement with the field data, whereas the constant vertical eddy viscosity model overestimates the wave length of the sand waves considerably.

The spatially and temporally variable vertical eddy viscosity caused much smaller growth rates for long sand waves compared to stability sand wave models, in which the vertical eddy viscosity is time independent. However, both for stability sand wave models and the k–ε turbulence model the growth rates for long sand waves were still positive. Future research will study whether the inclusion of suspended sediment in combination with a k–ε turbulence model will lead to negative growth rates for long sand waves.

Acknowledgements

This work is part of the PhD research of the first author, which is co-supported by the Dutch Technology Foundation STW, applied science division of NWO and the Technology Program of the Dutch Ministry of Economic Affairs. Fenneke Sterlini is acknowledged for providing the model output from the nonlinear stability sand wave model used for the intercomparison with our model. Deltares is acknowledged for funding part of the research and making its Delft3D software available.

References

Bagnold, R.A., 1956. The flow of cohesionless grains in fluids. Proceedings of the Royal Society Philosophical Transactions London 249, 71–81.
Besio, G., Blondeaux, P, Frisina, P., 2003. A note on tidally generated sand waves. Journal of Fluid Mechanics 485, 171–190.
Besio, G., Blondeaux, P., Brocchini, M., Vittori, G., 2004. On the modelling of sand wave migration. Journal of Geophysical Research 109, 1–13.
Besio, G., Blondeaux, P., Vittori, G., 2006. On the formation of sand waves and sand banks. Journal of Fluid Mechanics 557, 1–27.
Besio, G., Blondeaux, P., Brocchini, M., Hulscher, S.J.M.H., Idier, D., Knaapen, M.A.F., Németh, A.A., Roos, P.C., Vittori, G., 2008. The morphodynamics of tidal sandwaves: a model overview. Coastal Engineering 55, 657–670.
Blondeaux, P, Vittori, G., 2005a. Flow and sediment transport induced by tide propagation. 1. The flat bottom case. Journal of Geophysical Research 110, C07020.
Blondeaux, P, Vittori, G., 2005b. Flow and sediment transport induced by tide propagation. 2. The wavy bottom case. Journal of Geophysical Research 110, C08003.

Borsje, B.W., De Vries, M.B., Bouma, T.J., Besio, G., Hulscher, S.J.M.H., Herman, P.M.J., 2009. Modelling bio-geomorphological influences for offshore sand waves. Continental Shelf Research 29, 1289–1301.
Burchard, H., Craig, P.D., Gemmrich, J.R., van Haren, H., Mathieu, P.-P., Meier, H.E.M., Nimmo Smith, W.A.M., Prandke, H., Rippeth, T.P., Skyllingstad, E.D., Smyth, W. D., Welsh, D.J.S., Wijesekera, H.W., 2008. Observational and numerical modeling methods for quantifying coastal ocean turbulence and mixing. Progress in Oceanography.
Cherlet, J., Besio, G., Blondeaux, P., van Lancker, V., Verfaillie, E., Vittori, G., 2007. Modeling sand wave characteristics on the Belgian Continental Shelf and in the Calais–Dover Strait. Journal of Geophysical Research 112, C06002, http://dx.doi.org/10.1029/2007/JC004089.
Deltares, 2013. User manual Delft-3D FLOW, Deltares (⟨www.deltares.nl⟩), Delft, The Netherlands.
Dodd, N., Blondeaux, P., Calvete, D., De Swart, H., Falques, A., Hulscher, S.J.M.H., Rozynski, G., Vittori, G., 2003. The use of stability methods for understanding the morphodynamical behaviour of coastal systems. Journal of Coastal Research 19, 849–865.
Dorst, L.L., Roos, P.C., Hulscher, S.J.M.H., Lindenbergh, R.C., 2009. The estimation of sea floor dynamics from bathymetric surveys of a sand wave area. Journal of Applied Geodesy 3 (3), 97–120.
Fredsøe, J., Deigaard, R., 1992. Mechanics of Coastal Sediment Transport. World Scientific.
Gerkema, T., 2000. A linear stability analysis of tidally generated sand waves. Journal of Fluid Mechanics 417, 303–322.
Hulscher, S.J.M.H., 1996. Tidal-induced large-scale regular bed form patterns in a three-dimensional shallow water model. Journal of Geophysical Research C9 (101), 20727–20744.
Hulscher, S.J.M.H., Van den Brink, G.M., 2001. Comparison between predicted and observed sand waves and sand banks in the North Sea. Journal of Geophysical Research C5 (106), 9327–9338.
Huntley, D.A., Huthnance, J.M., Collins, M.B., Liu, C.L., Nicholls, R.J., Hewitson, C., 1993. Hydrodynamics and sediment dynamics of North Sea sand waves and sand banks,. Philosophical Transactions of the Royal Society of London, Series A 343, 461–474.
Knaapen, M.A.F., Hulscher, S.J.M.H., 2002. Regeneration of sand waves after dredging. Coastal Engineering 46, 277–289.
Komarova, N.L., Hulscher, S.J.M.H., 2000. Linear instability mechanisms for sand wave formation. Journal of Fluid Mechanics 413, 219–246.
Lesser, G., Roelvink, J., van Kester, J., Stelling, G., 2004. Development and validation of a three-dimensional morphological model. Coastal Engineering 51, 883–915.
McCave, I.N., 1971. Sand waves in the North Sea off the coast of Holland. Marine Geology 10, 199–225.
Németh, A.A., Hulscher, S.J.M.H., De Vriend, H.J., 2002. Modelling sand wave migration in shallow shelf seas. Continental Shelf Research 22, 2795–2806.
Németh, A.A., Hulscher, S.J.M.H., De Vriend, H.J., 2003. Offshore sand wave dynamics, engineering problems and future solutions. Pipeline and Gas Journal 230, 67–69.
Németh, A.A., Hulscher, S.J.M.H., Van Damme, R.M.J., 2007. Modelling offshore sand wave evolution. Continental Shelf Research 27, 713–728.
Rodi, W., 1984. Turbulence Models and Their Application in Hydrodynamics—A State of the Art Review. Univ. of Karlsruhe, Karlsruhe, Germany.
Sekine, M., Parker, G., 1992. Bed-load transport on transverse slope. Journal of Hydraulic Engineering 118, 513–535.
Sterlini, F.M., Hulscher, S.J.M.H., Hanes, D.M., 2009. Simulating and understanding sand wave variation: a case study of the golden gate sand waves. Journal of Geophysical Research 144 (F02007).
Terwindt, J.H.J., 1971. Sand waves in the Southern Bight of the North Sea. Marine Geology 10, 51–67.
Tonnon, P.K., van Rijn, L.C., Walstra, D.J.R., 2007. The morphodynamic modelling of tidal sand waves. Coastal Engineering 54, 279–296.
Van den Berg, J., Sterlini, F., Hulscher, S.J.M.H., Van Damme, R., 2012. Non-linear process based modelling of offshore sand waves. Continental Shelf Research 37, 26–35.
Van Dijk, T.A.G.P., Kleinhans, M.G., 2005. Processes controlling the dynamics of compound sand waves in the North Sea, Netherlands. Journal of Geophysical Research 110, 1–15.
Van Santen, R.B., de Swart, H.E., van Dijk, T.A.G.P, 2011. Sensitivity of tidal sand wave length to environmental parameters: a combined data analysis and modeling approach. Continental Shelf Research 31, 966–978.
Verboom, G.K., Slob, A., 1984. Weakly-reflective boundary conditions for two-dimensional water flow problems. Advances in Water Resources 7, 192–197.